Journal of The
Electrochemical Society

Pouch Versus Press Cells—How Cell Configuration Dictates Low-Pressure Performance in Sulfide Solid-State Batteries

To cite this article: J. Schubert *et al* 2026 *J. Electrochem. Soc.* **173** 170519

Journal of The Electrochemical Society, 2026 **173** 170519

Pouch Versus Press Cells—How Cell Configuration Dictates Low-Pressure Performance in Sulfide Solid-State Batteries

J. Schubert,[1,2,=,z] S. Kremer,[1,2,=,z] J. Hubl,[1,2] P. Minnmann,[1,2] F. Rossi,[1,2] S. S. M. Ji,[3] F. H. Richter,[1,2,*] K. Hatzell,[4,*] J. K. Eckhardt,[2] A. Bielefeld,[1,2] and J. Janek[1,2,5,z]

[1]*Institute for Physical Chemistry, Justus-Liebig-University Giessen, Giessen 35392, Germany*
[2]*Center for Materials Research, Justus-Liebig-University Giessen, Giessen 35392, Germany*
[3]*Department of Mechanical and Aerospace Engineering, Princeton University, Princeton, NJ 08544, United States of America*
[4]*Andlinger Center for Energy and Environment, Princeton University, Princeton, NJ 08540, United States of America*
[5]*BELLA, Institute for Nanotechnology, Karlsruhe Institute of Technology, Karlsruhe 76021, Germany*

Impressive electrochemical performance has been demonstrated with sulfide-based solid-state batteries. However, these results are predominantly obtained under high stack pressures—up to hundreds of MPa. While such conditions are valuable for probing fundamental material properties and intrinsic performance limits, the resulting cell metrics are not easily transferable to practical applications. Consequently, there is a growing imperative for application-oriented evaluation of SSBs under more realistic, low-pressure conditions in the single-digit MPa range. In this study, we demonstrate that the assessment of low-pressure performance can be significantly influenced by the chosen cell architecture. By comparing the cycling performance of sulfide-based SSBs—utilizing an NMC composite cathode and an In/(InLi)$_x$ anode with argyrodite-type Li_6PS_5Cl as electrolyte—in both pouch-cell and press-cell configurations, we reveal significant discrepancies in electrochemical performance at stack pressures ranging from 0 MPa to 25 MPa. Notably, the developed pouch cells exhibit superior electrochemical performance at low stack pressures of 1 MPa compared to their press-cell counterparts despite the same materials used. Using three-electrode pouch cells, we identify In/(InLi)$_x$ anode delamination as a primary low-pressure failure mechanism. Overall, our findings emphasize that a realistic assessment of SSB cell performance requires cell architectures that mirror targeted applications.

[DOI: 10.1149/1945-7111/aea0a2]

Manuscript submitted July 21, 2026; revised manuscript received August 19, 2026. Published September 8, 2026.

Supplementary material for this article is available online

Solid-state batteries (SSBs) emerge as an attractive alternative to conventional liquid electrolyte-based lithium-ion batteries due to their potential for increased energy density and enhanced safety.[1,2] While SSBs have already demonstrated impressive electrochemical performance under tailored operating conditions, research is now focusing on achieving such performance under more practical conditions.[3–5] In contrast to using liquid electrolyte, which easily wets the active materials, maintaining intimate contact in SSBs is more challenging.[6,7] Even when employing sulfide-based solid electrolytes (SEs), which offer favorable room-temperature malleability and higher ionic conductivity compared to oxides, interface contact inevitably deteriorates as the active material undergoes volumetric changes during (de-)lithiation.[8–12] To counteract this contact loss, stack pressures up to hundreds of MPa are typically applied.[13,14] While such conditions are valuable for probing fundamental material properties and intrinsic performance limits, the resulting cell metrics are not directly transferable to practical operating conditions.

Consequently, recent studies have begun to evaluate SSB performance under reduced stack pressure. For example, Gao et al. studied the performance of sulfide-based composite positive electrodes (hereafter referred to as cathode) of different compositions at low stack pressures of 2 MPa.[15] Using Li_3InCl_6 as catholyte, $LiNi_{0.83}Co_{0.11}Mn_{0.06}O_2$ as cathode active material (CAM), an Li_6PS_5Cl separator and an In/(InLi)$_x$ negative electrode (hereafter referred to as anode), they obtained a discharge capacity of around 100 mAh g^{-1} after 50 cycles with a charge and discharge rate of 0.3C at 80 °C. By reducing the cut-off potential from 4.4 V vs. Li$^+$/Li to 4.2 V vs. Li$^+$/Li, they could increase the capacity retention to around 120 mAh g^{-1}. While this demonstrates that cell operation at relatively low stack pressure is feasible, the beneficial effect of a reduced cut-off potential, i.e. reduced volumetric changes of the CAM, underscores the importance of maintaining interfacial contact within the composite. To mitigate chemo-mechanical degradation, high stack pressures of more than 50 MPa are therefore still predominantly used when a satisfactory cathode performance is the main interest.[14]

Yet, the used stack pressure may differ considerably when the anode is the primary focus of investigation.[16–18] With a lithium metal anode, lower pressures are usually applied as excessive pressure can accelerate lithium creep through the separator, thereby increasing the risk of dendrite formation.[19,20] Conversely, if the pressure is too low, pore formation at the lithium metal–SE interface leads to contact loss during electrodissolution (i.e. discharging of the battery).[16,19] Furthermore, stack pressure was shown to influence interphase formation in SSBs.[21] Similarly, careful attention to stack pressure requirements is essential for silicon-based concepts. Severe microstructural degradation caused by the large volume changes of silicon upon (de-)lithiation, are—similar to the composite cathode—often mitigated by high stack pressures of 50 MPa and more.[22–24]

Clearly, the identification of viable stack pressure conditions for SSB electrodes becomes challenging when cathode and anode performances differ substantially within the investigated pressure range. For investigation of the cathode under low operating pressure, $Li_4Ti_5O_{12}$ as zero-strain material has been employed in composite anodes.[25] In such a cell, assessing the influence of stack pressure on the cathode performance is facilitated as chemo-mechanical degradation of the anode can be assumed to be negligible. In a different approach, Doerrer et al. made use of a lithium metal

[=] These authors contributed equally to this work.
[*] Electrochemical Society Member.
[z] E-mail: johannes.schubert@phys.chemie.uni-giessen.de; sascha.kremer@phys.chemie.uni-giessen.de; juergen.janek@phys.chemie.uni-giessen.de

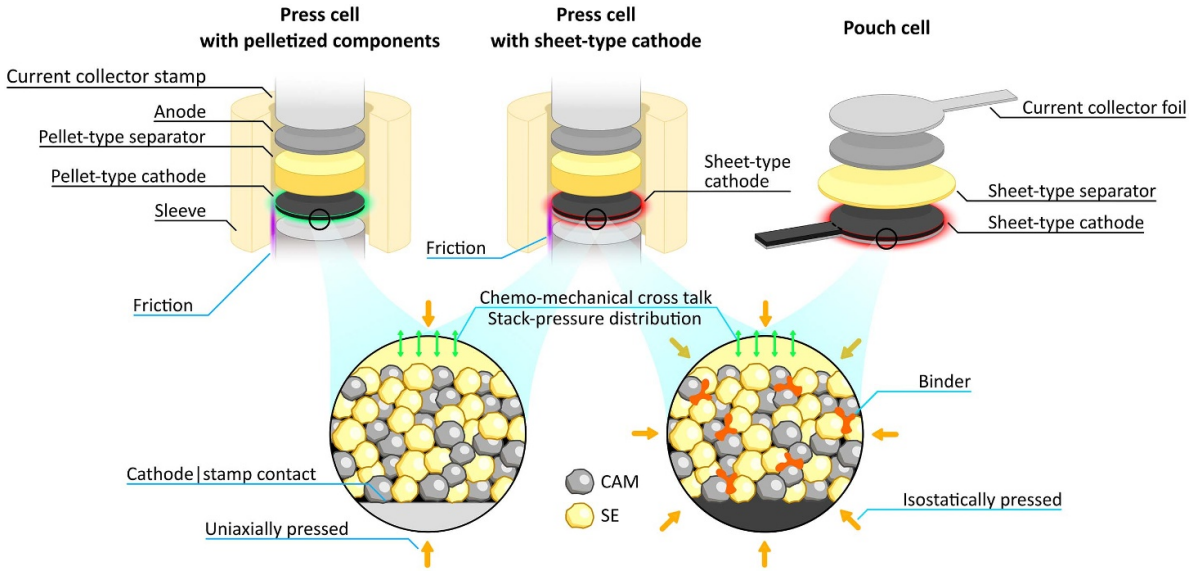

Figure 1. Schematic illustration of cell configurations commonly employed in SSB research and employed in this study. The performance of press cells with pelletized components and pouch cells with sheet-type components may be influenced by distinct factors (indicated by blue lines). A press cell containing a sheet-type cathode may exhibit mixed characteristics of press cells and pouch cells.

reference electrode to study the fast-charging capabilities of a $LiNi_{0.83}Co_{0.11}Mn_{0.06}O_2$:$Li_6PS_5Cl$ composite cathode under a low stack pressure of 0.2 MPa.[26] In addition, the authors used a specifically designed setup with which they could apply a higher pressure of 10 MPa alone onto the $In/(InLi)_x$ counter electrode. In this configuration and with optimized cut-off potentials, a capacity retention of 81% was demonstrated after 3000 cycles at an asymmetric charge/discharge rate of 4.8 C and 1.6 C at 30 °C.

These studies, as well as the vast amount of literature on sulfide-based SSBs in general, rely on laboratory-scale "press cells," which employ thick cell housings and rigid metal pistons as current collectors (see Fig. 1 "Press cell").[27] In such configurations, friction between the pistons and the cell housing can lead to significant deviations between externally applied and internally experienced pressure (especially at low stack pressure). Moreover, those cells may suffer from a poor current collector-electrode contact as the current collectors cannot adapt to the electrode surface.[28,29] In contrast, in SSB pouch cells that utilize thin, flexible, sheet-type components, friction at the cell edges does not occur and electrodes are directly coated onto current collectors, enabling improved interfacial conformality.[30,31] However, transitioning to pouch cell architectures introduces additional challenges, including the need for binders and advanced fabrication techniques such as tape casting, calendaring, and isostatic pressing (see Fig. 1 "Pouch cell"). Due to their adhesive and elastic properties, binders are believed to mitigate mechanical degradation and functionalized binders have been shown to enhance the low-pressure performance of cathodes.[32–35] Similarly, the densification procedure influences residual porosity and material contact and by that potentially the microstructural integrity of the composite.[36]

Consequently, the properties of press and pouch cells may differ considerably, particularly at low stack pressures. Yet, although SSB commercialization will require the fabrication of pouch cells, the systematic investigation of their performance under practical stack pressures has yet received limited attention. Chen et al. observed a considerable drop in reachable capacity and deterioration of the long-term cycling stability in $Si|Li_6PS_5Cl|LiNi_{0.8}Co_{0.1}Mn_{0.1}O_2$ pouch cells when isostatic stack pressure was reduced from 5 MPa to 1 MPa.[37] Using a three-electrode setup, they attributed this decline to an impedance increase at both the cathode and the silicon anode caused by contact loss to the solid electrolyte. While pouch cell cycling in a similar pressure range has also been conducted in other studies, the primary objective of these experiments is often the demonstration of a practical cell concept rather than a systematic evaluation of pressure-dependent limitations.[3,38–41] Hence, for these cells high-capacity Li-and Si-based concepts are typically used at the anode side, complicating the independent assessment of the acceptable stack pressure requirements for anode and cathode. In addition, this impedes direct comparison with the extensive body of press cell literature, in which an $In/(InLi)_x$ counter electrode is commonly employed. Therefore, the transferability of results obtained from press cells to pouch cells remains unclear.

In this work, we address this by systematically investigating the influence of stack pressure on sulfide-based SSB performance, with particular emphasis on differences between press cell and pouch cell configurations at low stack pressures. To this end, we examine three cell architectures: (*i*) a press cell with pellet-type cathode and pellet-type separator, (*ii*) a press-cell with sheet-type cathode and pellet-type separator, and (*iii*) a pouch cell with sheet-type cathode and sheet-type separator. As solid electrolyte and cathode active material we use commercially available Li_6PS_6Cl and $LiNi_{0.83}Co_{0.11}Mn_{0.06}O_2$, respectively. An $In/(InLi)_x$ anode is employed as a model counter electrode since it is well-established and the superior performance of indium at low stack pressures compared to other metal anodes has recently been demonstrated.[42] Additionally, three-electrode pouch cells are constructed to identify the dominant mechanisms contributing to long-term capacity fading under low stack pressure.

We demonstrate that the developed pouch cells exhibit substantially improved electrochemical performance at low stack pressures (0 MPa and 1 MPa) compared to press cell configurations. In both cell types and in accordance with literature reports, capacity fading at zero stack pressure is primarily governed by contact loss at the $In/(InLi)_x$ anode interface, while the composite cathode seems to remain comparatively stable. Overall, our findings emphasize that a realistic assessment of SSB cell performance requires practical cell architectures that mirror targeted applications. Low-pressure performance in press cell type setups might be significantly impacted by setup limitations (e.g. unavoidable friction with the cell housing) rather than intrinsic pressure limitations of the cell.

Experimental

Preparation of separator and cathode sheets.—Separator and cathode films were prepared using a tape casting process. For this, a binder solution, which was used for both films, was prepared by dissolving 5 wt.-% polyisobutylene (Oppanol N-150®, BASF) in ortho-xylene (99%, extra dry, Thermo Fisher Scientific).

For preparation of the separator, 1.67 g of the pre-mixed binder solution was added to 2 g of Li_6PS_5Cl (LPSCl) solid electrolyte powder (D_{50} = 5 μm, POSCO) and mixed at 2000 rpm for 5 min in a centrifuge mixer (Speedmixer DAC 150, Hauschild). The resulting dispersion was then further homogenized for 1 min using an ultrasonicator (UP100H, Hielscher Ultrasonics). Three zirconia balls (5 mm diameter) and 1 ml xylene were added, and the dispersion was again mixed at 2000 rpm for 5 min. Subsequently, additional 0.3 ml of xylene were added followed by a final mixing step under identical conditions. Using a doctor blade (1803/60/4, BEVS Industrial Co.), the dispersion was then coated onto a siliconized polymer foil (PPI Adhesive Products) with a wet film thickness of 600 μm. After drying under vacuum at 80 °C for 12 h, the film was sealed in a pouch bag and isostatically compressed at 350 MPa for 5 min. This resulted in a ca. 110 μm thick freestanding film with a binder content of 4 wt.-% and an ionic conductivity of about 0.5 mS cm^{-1} (at 25 °C and a stack pressure of 25 MPa).

For the cathode, a dry powder mixture was prepared in an initial step. $LiNi_{0.82}Mn_{0.07}Co_{0.11}O_2$ (NCM, D_{50} = 3–5 μm, MSE Supplies) and LPSCl (D_{50} = 0.7 μm, POSCO) were mixed with a weight ratio of 80:20 in a batch mill (Tube Mill, IKA-Werke) for 4 min with 15 000 rpm. To avoid comminution of the conductive additive during high frequency milling, 1.5 wt.-% of carbon nanofibers (Sigma-Aldrich, product number 719781) were introduced in a subsequent step and the mixture was thoroughly homogenized by hand in an agate mortar for 10 min. Afterwards, 1.5 ml of xylene were added to 2 g of the mixture which was then mixed at 2000 rpm for 5 min and ultrasonicated for 2 min. Three zirconia balls and 0.61 g of the pre-mixed binder solution (corresponding to 1.5 wt.-% binder in the cathode) as well as 0.6 ml of xylene were introduced in two subsequent steps, and each was followed by mixing and ultrasonication identical to the first step. A wet cathode film with a thickness of 300 μm was then cast onto a carbon-coated Al foil (17 μm thickness, PI-KEM), which served as current collector. The final drying and densification of the cathode films was identical to that of the separator film. All preparation steps were carried out under argon atmosphere if not stated otherwise.

Preparation of pouch cells.—Cathodes were punched from the cathode film into a half-dumbbell shape, featuring a circular active area (15 mm diameter) and a narrow rectangular extension to which tabs can be attached (see Fig. 1). Circular separator discs (18 mm diameter) were punched from the separator film and placed on the cathode. For the $In/(InLi)_x$ alloy anode, first, an indium disc (15 mm diameter, 100 μm thickness, ChemPur) and then a lithium disc (9 mm diameter, 100 μm thickness, China Energy Lithium Co.) were stacked on the separator. The cell stack was then sealed in a pouch bag and isostatically pressed at 350 MPa and room temperature for 15 min. After pressing, the cell was removed from the pouch bag and a stainless-steel current collector (20 μm thickness, GoodFellow) with a half-dumbbell shape was positioned on the anode. Finally, aluminum tabs were glued to the current collectors, and the cell was again vacuum sealed in a pouch bag.

Three-electrode cells were assembled based on a configuration reported by Sedlmeier et al., in which a lithiated gold wire is sandwiched between two separator sheets and serves as reference electrode.[43] For this, the polyester coating of an insulated gold wire (50 μm diameter gold wire, 7 μm polyester coating, Goodfellow Cambridge Limited) was removed at the tip in an initial step. To integrate the gold wire into the cell, the two-electrode setup as described above was adjusted, and two separator discs were used. The tip of the gold wire was then centered between the separator discs. The dimensions of the components and the remaining cell preparation were identical to the two-electrode cells. In the last step, the gold wire was electrochemically lithiated with a current of 250 nA for 12 h leading to the formation of a Li–Au alloy phase which provided a stable potential of 0.31 V vs. Li^+/Li.

Preparation of press cells and sheet-type press cells.—SSB cells with pellet-type and sheet-type composite cathodes were assembled in an in-house developed casing already used in other studies and described in detail by Zhang et al.[27] For preparation of the separator, 60 mg of LPSCl (D_{50} = 5 μm) were loaded into a PEEK sleeve (10 mm diameter) and compacted between two steel pistons using a hand press. For the cathode, either a composite powder mixture (a) or a sheet (b) was integrated as follows:

a) First, a dry powder mixture consisting of NCM, LPSCl (D_{50} = 0.7 μm), and carbon nanofibers was prepared with a weight ratio of 80:20:1.5. Three zirconia balls (5 mm diameter) were added to 100 mg of material, and the mixture was agitated for 30 min with an oscillation frequency of 30 Hz using a mini vibrating mill (Pulverisette 23, Fritsch).[44] Subsequently, 9.81 mg of the powder (corresponding to an area capacity of 2 mAh cm^{-2}) were homogeneously distributed on the separator and a carbon-coated aluminum foil disc (9.6 mm diameter) was added.
b) A cathode disc (9.6 mm diameter) was punched from the cathode films and placed on the separator.

For the anode, an indium disc (9 mm diameter) and a lithium disc (6 mm diameter) were placed on the separator. Finally, the cell was uniaxially pressed at 375 MPa for 3 min.

Electrochemical characterization.—To test the long-term cycling performance, an initial formation cycle was conducted with 0.1 C (1 C = 200 mA g^{-1}) between 2.0 and 3.7 V using a BCS-805 battery cycler (BioLogic). When the potential reached 3.3 V, 3.7 V, and 2.0 V, it was held at that potential until the current dropped below 0.02 C. After the constant-potential step at 3.3 V, a potentiostatic impedance measurement was performed in a frequency range from 10 kHz to 100 mHz with an amplitude of 10 mV. Following the formation cycle, the cells were galvanostatically cycled with 1 C without further constant-potential steps. At the cut-off potentials the potential was allowed to relax for 10 min. Three-electrode cells were cycled with the same protocol using a VMP-300 potentiostat (BioLogic), except that the upper frequency limit was increased to 3 MHz. To test the rate performance, the C-rate was stepwise decreased from 2 C to 0.1 C followed by two check-up steps at 2 C and 1 C and final step with 4 C.

All cells were either cycled without additional stack pressure or at 1 MPa or 25 MPa and at 25 °C or 40 °C. The stack pressure is calculated using the electrode areas. For pressure application, a custom-made frame was used equipped with a force sensor as well as a spring to compensate for pressure relaxation.

Additionally, two-electrode pouch cells were evaluated under varying pressure conditions during the cycling experiment at 25 °C and 40 °C using a CompreDrive automatic press (rhd instruments) and an SP-200 potentiostat (BioLogic). First, a formation cycle was carried out as described above which was followed by six cycles with 1 C at 25 MPa. The pressure was then stepwise decreased to 1 MPa and at each pressure one cycle was conducted with 1 C. After reaching 1 MPa the pressure was either stepwise increased back to 25 MPa or an additional formation cycle was performed at 1 MPa before the pressure was increased again.

Preparation of cross sections.—Cross sections were prepared using a XEIA3 Xe-plasma focused ion beam-scanning electron microscope (FIB-SEM, Tescan). All sample transfers were carried out under an inert Ar-atmosphere or vacuum using a VCT transfer module (Leica).

Results

Cycling performance of press and pouch cells at different stack pressure.—To assess the differences between press cells containing pelletized components and pouch cells containing sheet-type components, the long-term cycling stability and rate capability of these cells were evaluated at stack pressures of 25 MPa, 1 MPa and 0 MPa (where 0 MPa denotes the absence of additional applied stack pressure other than atmospheric pressure). While some differences may be inherent to each cell configuration, others may stem solely from the fabrication of sheet-type components, such as isostatic densification or the presence of a polymer binder. To decouple these effects, a second press cell configuration was tested in which the pellet-type cathode was substituted by a sheet-type cathode (see Fig. 1 "Press cell with sheet-type cathode"). For evaluation of the cycling stability, cells were subjected to continuous cycling at 1 C, preceded by a formation cycle at 0.1 C and with intermediate constant-potential holds at 3.3 V vs. In/InLi and at the cut-off potentials. The low-rate formation cycle with constant-potential holds serves a dual purpose: it allows an assessment of the CAM utilization, and in addition, it ensures an initial comparable and high state-of-charge (SoC) for all cathodes. The latter is essential for comparison as the overpotentials due to kinetic limitations may vary for the three cell configurations resulting in diverging maximal reached SoCs and, consequently, differing degrees of chemo-mechanical degradation. Moreover, the elevated SoC maximizes chemo-mechanical stress during the formation cycle, thereby amplifying differences in chemo-mechanical degradation between the different cell configurations. To ensure reproducibility of the results, measurements were repeated three times at 25 °C for each cell configuration and stack pressure.

Figures 2a–2c show the potential profiles, i.e. profiles of the potential difference, during the formation cycle for the three cell configurations at 25 MPa, 1 MPa and 0 MPa stack pressure. At 25 MPa, the charge and discharge curves display a similar profile for all configurations exhibiting a characteristic plateau at around 3.55 V associated with the H_2–H_3 transformation in Ni-rich NCM.[45] The delivered charge and discharge capacities are virtually identical and in the range of the theoretical capacity of the used NCM (200 mAh g^{-1}). This confirms that a high CAM utilization can initially be achieved with both press cells and pouch cells, indicating effective mixing through dry powder and slurry-based electrode preparation, respectively.[44] For pouch and press cells with pellet-type cathode, a reduction of the stack pressure from 25 MPa to 1 MPa does not result in a considerable decrease of the attainable capacity at 0.1 C and the H_2–H_3 transformation is still visible in both potential profiles. While charge and discharge curves of these configurations are similar at 25 MPa and 1 MPa, the press cell with sheet-type cathode exhibits a higher overpotential and longer constant-potential holds suggesting slower kinetics. Compared to a stack pressure of 1 MPa, releasing the stack pressure entirely has a minor influence on the potential profiles, and all cell configurations retain a high discharge capacity of more than 180 mAh g^{-1} after the constant-potential hold. Overall, the formation cycles show that press cells and pouch cells initially deliver a similar electrochemical performance, even when cycled without stack pressure, if the C-rate is low, i.e. if kinetics plays a minor role.

In contrast, significant differences between the three cell configurations become apparent at different stack pressures during continuous cycling with 1 C (see Figs. 2d–2f). At 25 MPa, pouch and press cells reach comparable capacities of approximately 125 mAh g^{-1} in the initial cycles. While the capacity of the pouch cells remains almost constant and above 120 mAh g^{-1} after 100 cycles, the press cells with pellet-type cathode show more pronounced capacity fading, dropping below 100 mAh g^{-1}. Increasing the stack pressure of press cells with pellet-type cathode to 75 MPa leads to improved capacity retention, corroborating chemo-mechanical degradation as the dominant degradation mechanism (see Fig. S1).

Notably, press cells with sheet-type cathodes exhibit substantially lower capacities compared to the other configurations, not exceeding 100 mAh g^{-1}. As all configurations show comparable CAM utilization in the formation cycle, this is ascribed to kinetic losses due to the blocking of charge transport paths by microstructural defects, which causes higher tortuosity, and lower effective conductivities. This is supported by cross sectional SEM images of *uncycled* sheet-type cathodes of these cells that show a highly degraded composite cathode microstructure with fractures formed within the SE phase, secondary CAM particles, and at the CAM|SE interface (see Fig. S2). These fractures probably originate from over-pressurization caused by isostatic densification during cathode sheet preparation followed by uniaxial pressing of the cell stack during assembly of the press cell. Isostatic densification leads to a highly densified composite, likely altering its response to subsequent uniaxial pressing. The composite cannot accommodate the applied stress through further densification, resulting primarily in elastic deformation. Upon pressure release, this induces a springback effect detrimental to the microstructural integrity of the composite.[46–48]

At 1 MPa, the performance of pouch and press cells differ with respect to initially attainable capacity, and more pronouncedly, long-term capacity retention. Compared with 25 MPa, the pouch cell capacity in the first cycles decreases by approximately 30% to 90 mAh g^{-1}, whereas the capacity of the press cells with pellet-type cathode decreases by approximately 60% to 50 mAh g^{-1}. Interestingly, the variation between the press cells increases at 1 MPa, which may indicate a more prominent role of friction at low stack pressures. While some friction arises from the rubber sealing rings that isolate the cell from ambient air, a potentially greater contribution may stem from In/$(InLi)_x$ residues which can be pressed between steel piston and sleeve during cell preparation (see Fig. S3). In consequence, the actual stack pressure experienced by the cell stack may deviate from the nominally applied value, and—as these friction forces can vary between individual cells—the spread of results may be higher. Upon further cycling, the capacity of the press cells diminishes to 0 within the first 50 cycles, proving rapid degradation. The pouch cells, by contrast, demonstrate a remarkable long-term cycling stability and around 80 mAh g^{-1} are still achieved after 100 cycles. We further like to note, that a pouch cell cycled at 1 C and 40 °C, which is a reasonable operating temperature for practical applications, also exhibits stable cycling after reaching a plateau at a capacity of 130 mAh g^{-1} (see Fig. S4). In agreement with the results at 25 MPa, the press cells with sheet-type cathodes exhibit a significantly inferior cycling performance, practically preventing low stack pressure operation. Unlike at high stack pressure, where fractures present in the cathode may be partially closed, low stack pressures are insufficient to do so, resulting in high overpotentials.

Cycling without stack pressure further demonstrates the superior performance of the pouch cells. Even though the complete removal of stack pressure leads to a considerable capacity decrease, approximately 25 mAh g^{-1} can be delivered after 100 cycles with no indication of substantial further decay. A stabilization of the capacity is also observed in an analogous experiment conducted at a C-rate of 0.5 C, with slightly faster fading in the initial cycles due to the higher capacities delivered at this C-rate and the correspondingly higher chemo-mechanical stress (see Fig. S5). The capacity of the press cells with pellet-type cathode, on the other hand, quickly drops from initially 10 mAh g^{-1} to 0. We note that friction is of particular importance at zero stack pressure. Without additional stack pressure the current collector in a press cell, i.e. the steel stamp, cannot follow the cathode upon volume contraction, resulting in a lower effective stack pressure or even complete contact loss. This is different compared to a pouch cell, where the cell stack always experiences at least atmospheric pressure.

At low stack pressures, cell performance limitations attributable to the In/$(InLi)_x$ anode must be considered. In SSB press cells containing an indium metal anode and NCM622 as CAM, Wang et al. reported a decrease of the cell capacity below 2 MPa due

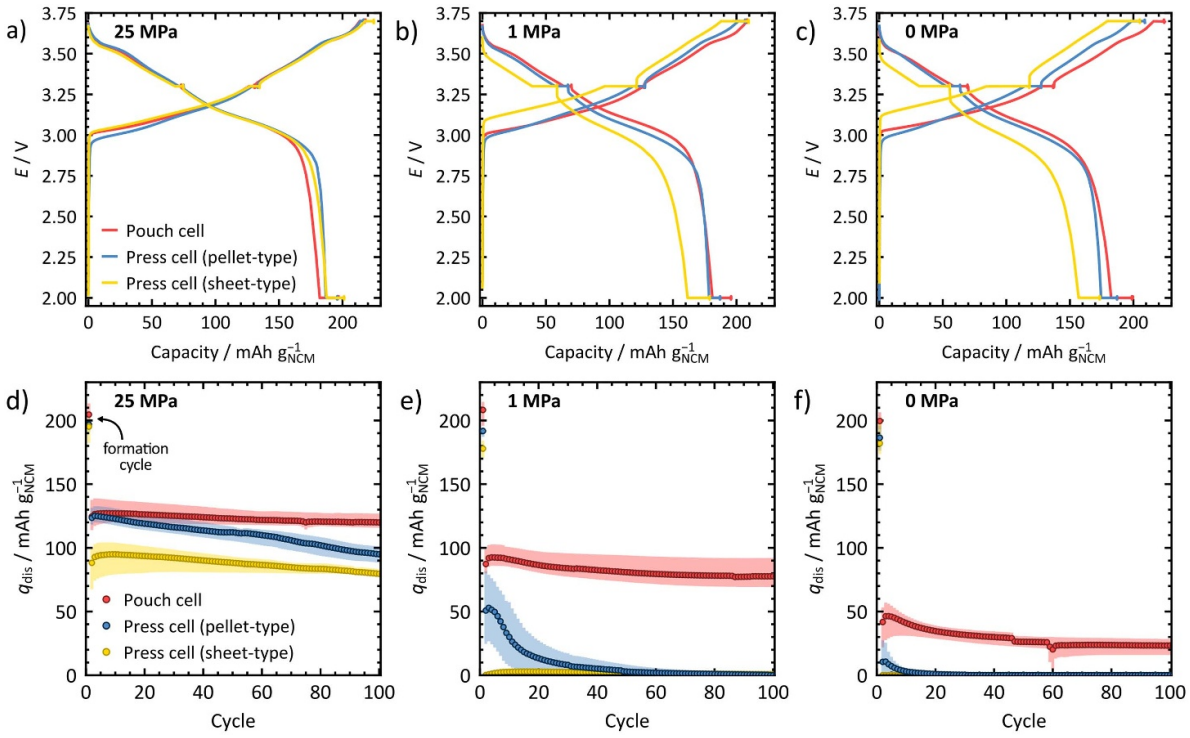

Figure 2. Long-term cycling of In/InLi|LPSCl|NCM press cells with pellet-type cathode (blue), press cells with sheet-type cathode (yellow) and pouch cells (red) with a stack pressure of 25 MPa, 1 MPa and 0 MPa. (a)–(c) Potential profiles of the formation cycle with a C-rate of 0.1 C and intermediate constant-potential steps. (d)–(f) Evolution of the discharge capacity q_{dis} during cycling with 1 C. The temperature was 25 °C and the areal capacity was 2 mAh cm^{-2}. The circles are the average of three cells, and the shaded areas indicate minimum and maximum values of these cells. The artifacts after 47 and 59 cycles for the pouch cells at 0 MPa were caused by a software failure of the potentiostat. Potential profiles of all 1 C cycles are depicted in Fig. S7.

to pore formation and interfacial contact loss during dealloying.[42] Although the same In/(InLi)$_x$ anode was employed for all cell configurations to ensure a high comparability, configuration-specific factors may influence the cell performance. These include, e.g. an improved anode|separator interfacial contact through isostatic densification during pouch cell assembly, or inhomogeneous current distribution arising from a less planar interface between separator, anode and pelletized cathode, potentially affecting anode lithiation and delithiation (see Fig. S6).[49,50]

These configuration-specific differences are further supported by electrochemical impedance spectroscopy (EIS) measurements recorded after the 3.3 V constant-potential holds during the initial slow-rate formation cycle (see Fig. S8). Even at this early stage, a significant increase in the impedance contribution typically assigned to the anode is observed for the press cells when operated at low stack pressure. This strongly hints that the rapid capacity loss observed during continuous 1 C cycling in these cells is inherently tied to early contact loss at the anode interface. In the case of the pouch cells, while the overall impedance is also pressure-dependent, both the anode and cathode contributions appear to scale equally with pressure, indicating a much more balanced and mechanically robust interfacial contact across the entire cell.

Figure 3 shows the discharge capacity reached at C-rates between 0.1 C and 2 C for the three configurations at 25 MPa, 1 MPa and 0 MPa stack pressure. For this, the rate tests were conducted starting with high C-rates as preceding cycles with low C-rates, i.e. when a higher SoC is reached, may already result in chemo-mechanical degradation. This can lead to a misrepresentation of the rate capability and by that may complicate comparison, especially when cells are operated under challenging conditions, i.e. low stack pressure.

At 25 MPa and a C-rate of 0.1 C, all configurations reach similar discharge capacities in the range of 180–190 mAh g^{-1}. For pouch cells and press cells with pellet-type cathode, a stack pressure reduction to 1 MPa and 0 MPa leads to a minor decrease and approximately 170 mAh g^{-1} are reached for both pressures, whereas the capacities of the press cells with sheet-type cathode drop below 150 mAh g^{-1}. The obtained capacities are consistent with the capacities achieved during the formation cycles in the long-term cycling test and provide additional evidence for the conclusions presented above, i.e. if kinetic limitations are negligible, a high CAM utilization can be achieved with all three cell configurations at all stack pressures employed. The press cells with sheet-type cathode show higher overpotentials (see Fig. S9), which is caused by impeded charge transport due to a degraded cathode microstructure. At 25 MPa and higher C-rates the three configurations exhibit a similar capacity and approximately 60 mAh g^{-1} are reached at 2 C. At 1 MPa and 0 MPa, the pouch cells achieve the highest capacities, reaching approximately 20 mAh g^{-1} at 2 C, while zero capacity is delivered by the press cells with pellet and sheet-type cathodes.

Interestingly, compared to the long-term cycling test at 1 C, press cells with sheet-type cathode reach a higher capacity at all pressures. We attribute this to the absence of the formation cycle, preventing preceding microstructural degradation, which enables improved charge transport at high C-rates. Check-up cycles conducted with 1 C and 2 C after the rate test show reduced capacities for these cells, confirming ongoing degradation during the rate test, particularly at low rates (see Fig. S10). Generally, pouch and press cells exhibit comparable rate capabilities, which is in strong contrast to the observed pronounced differences of long-term cycling stability.

Microstructural evolution of press and pouch cells during cycling without stack pressure.—To assess the impact of long-term cycling on the microstructural evolution, partial cross sections of the composite cathodes were prepared from pouch cells and press cells with pellet-type cathode before cycling and after 100 cycles without stack pressure (see Fig. 4). Figures 4a and 4c show the

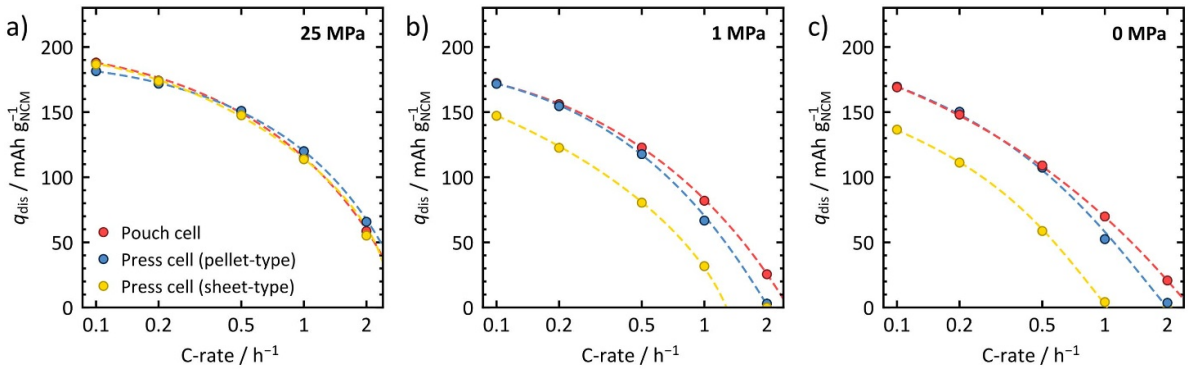

Figure 3. C-rate test of In/InLi|LPSCl|NCM press cells with pellet-type cathode (blue), press cells with sheet-type cathode (yellow) and pouch cells (red) with a stack pressure of (a) 25 MPa, (b) 1 MPa and (c) 0 MPa. The temperature was 25 °C and the areal capacity was 2 mAh cm^{-2} (calculated based on the theoretical specific capacity of the CAM). The depicted capacities are the average capacities at each C-rate step. The dashed line is provided as a guide to the eye. A comparable measurement for a press cell with pellet-type cathode at 75 MPa is depicted in Fig. S11.

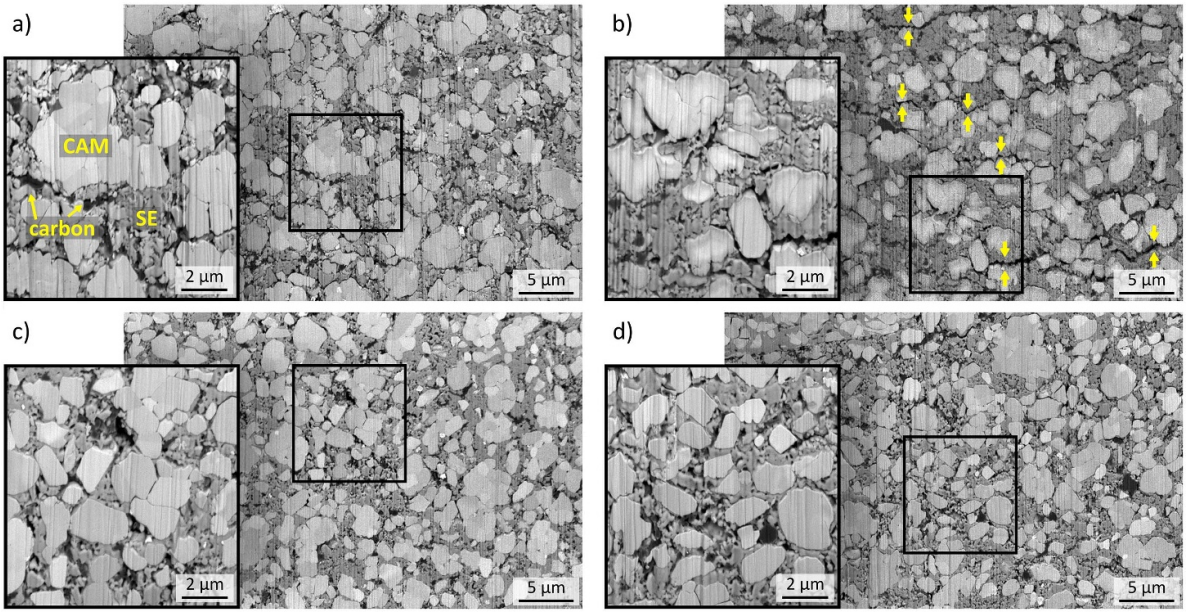

Figure 4. FIB-SEM images of composite cathodes. (a) Pouch cell, sheet-type cathode before cycling. (b) Pouch cell, sheet-type cathode after long-term cycling. (c) Press cell, pellet-type cathode before cycling. (d) Press cell, pellet-type cathode after long-term cycling. Fractures are indicated by yellow arrows. Cycling was performed at 1 C with 0 MPa stack pressure at 25 °C.

cathodes of the uncycled pouch cell and the uncycled press cell, respectively. In both cases, the SE is homogeneously distributed between the CAM particles, with no carbon fiber agglomerates and, in the case of the pouch cell, no binder agglomerates visible. This further confirms effective mixing of pellet-type and sheet-type composite cathodes, consistent with the findings from electrochemical characterization. Moreover, despite the distinct densification methods, i.e. isostatic or uniaxial pressing, inter-particle contacts appear intimate, and the residual porosity seems comparably low for both cathodes.[51] The differing electrochemical performance of pouch cells and press cells with pellet-type cathode, particularly at low stack pressures, is therefore unlikely to originate from different degrees of composite cathode densification. Importantly, signs of microstructural degradation prior to cycling, which may be induced by handling the sheet, cell fabrication, or sample preparation, cannot be observed.

After 100 cycles at 1 C without stack pressure, the pouch cell cathode exhibits fractures of several micrometers in length, propagating along CAM|SE interfaces and through the SE phase, with a preferential orientation parallel to the electrode plane (Fig. 4b). The formation of such mesoscopic fractures is likely driven by stress relief, which is facilitated perpendicular to the cell stack if no pressure is applied, i.e. the cell volume is unconstrained in this direction. Although contact loss at CAM|SE interfaces is expected to promote fracture formation, the predominantly intact interfacial contact suggests that CAM volume changes are primarily accommodated by mesoscopic fracture formation rather than interfacial delamination. Importantly, the preferential orientation of fractures may be particularly detrimental to ionic transport, as lithium ions must traverse the cathode thickness, and therefore, along a direction in which conduction pathways are most severely disrupted.

The pellet-type cathode of the press cells, in contrast, shows no obvious microstructural degradation after zero stack pressure long-term cycling despite rapid capacity fading. Moreover, the interfacial contact between cathode and separator as well as between cathode and current collector remains intact, as in the case of the pouch cell (see Fig. S6). This indicates the anode primarily drives capacity loss, leaving the cathode structurally intact due to a limited depth of charge and discharge.

Figure 5a shows the cross section of the anode|separator interface in the pouch cells prior to cycling, revealing close and conformal

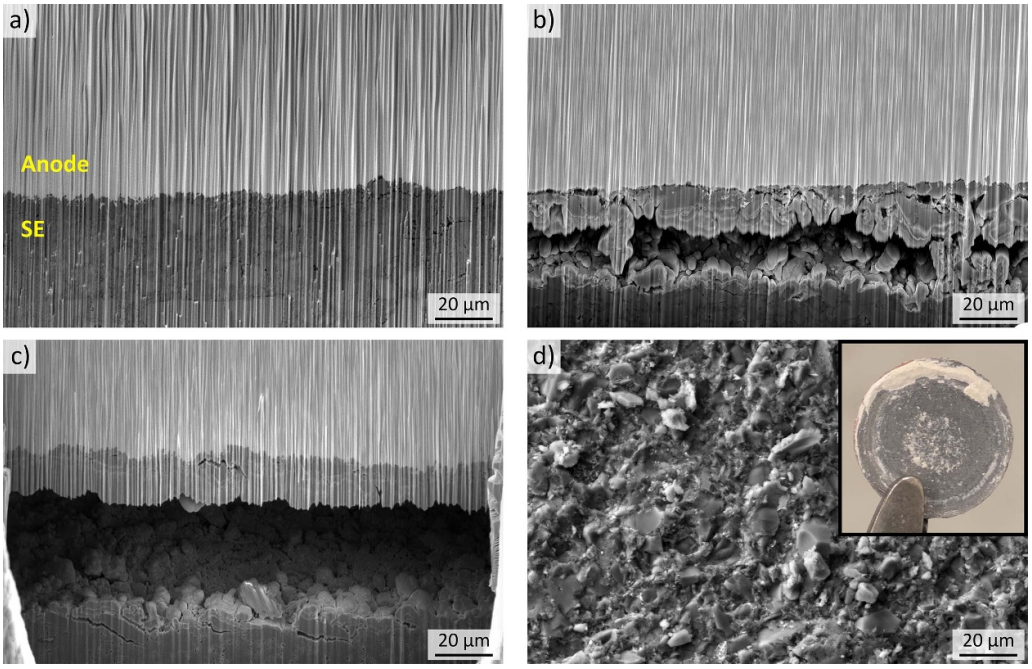

Figure 5. FIB-SEM images of the anode|separator interface of (a) pouch cell before cycling, (b) pouch cell after long-term cycling at 0 MPa, and (c) press cell before cycling. (d) Top-view SEM image of the anode (anode|separator interface) and corresponding photographic image after cycling.

interfacial contact. After cycling without stack pressure, a single large fracture near the interface is visible (see Fig. 5b), indicating microstructural degradation at the anode side as an additional contributor to capacity fading. Interestingly, delamination does not occur directly at the interface. Instead, a layer of SE particles remains adhered to the anode, suggesting strong anode|separator adhesion. This implies chemo-mechanical degradation within the separator layer near the interface, driven by anode volume changes and associated mechanical stresses, rather than by interfacial void formation due to lithium depletion during delithiation.

SEM images of the press cells' anode|separator interface reveal an anode that appears delaminated even prior to cycling. However, the high capacity achieved during the formation cycle and the recently reported significant reduction in interfacial impedance upon uniaxial pressing of In/$(InLi)_x$ anodes in press cells indicate that a robust initial anode|separator contact is, in fact, initially established.[52] Therefore, the observed delamination is likely a mechanical artifact caused by removing the sample from the press cell casing. Importantly, post-cycling cross-sections of this interface could not be prepared, as the anode immediately detached from the separator during cell disassembly (see Fig. 5d). We therefore attribute the poor long-term cycling stability of the press cells to contact loss at, or more precisely, immediately adjacent to, the anode|separator interface. Crucially, this degradation does not appear to stem from poor adhesion between separator and anode, but rather from a loss of SE|SE particle contact within the separator just beneath the interface.

Pouch cell performance under varying stack pressure, impact of temperature, and high SoCs.—Following the demonstration of superior pouch cell performance at low stack pressures, we investigated their performance under variable pressures in greater detail using a CompreDrive automatic press (Fig. 6a). The cycling experiments were conducted at 1 C. Starting with cycling at 25 MPa the stack pressure was first stepwise decreased to 1 MPa, followed by a stepwise increase back to 25 MPa. Prior to pressure variation, a formation cycle at 0.1 C and six subsequent cycles at 1 C were performed at 25 MPa to ensure a stabilization of the capacity.

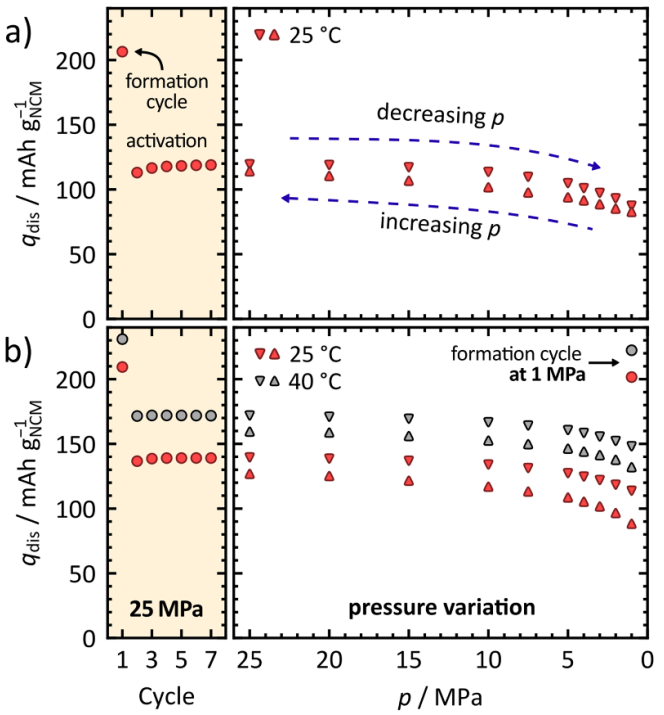

Figure 6. Pouch cell cycling tests with varying pressure at 1 C (a) without formation cycle at 1 MPa and (b) with formation cycle at 1 MPa. The areal capacity was 2 mAh cm^{-2}. Differences in the capacity obtained in (a) and (b) of the cells cycled at 25 °C are within the margin of error depicted in Fig. 2d. The downward-pointing triangles mark cycles during the pressure-decrease sequence and the upward-pointing triangles mark cycles during the pressure-increase sequence.

Upon reducing the stack pressure from 25 MPa to 1 MPa, the capacity decreases monotonically by approximately 30%, with roughly half of the total loss occurring at pressures below 5 MPa.

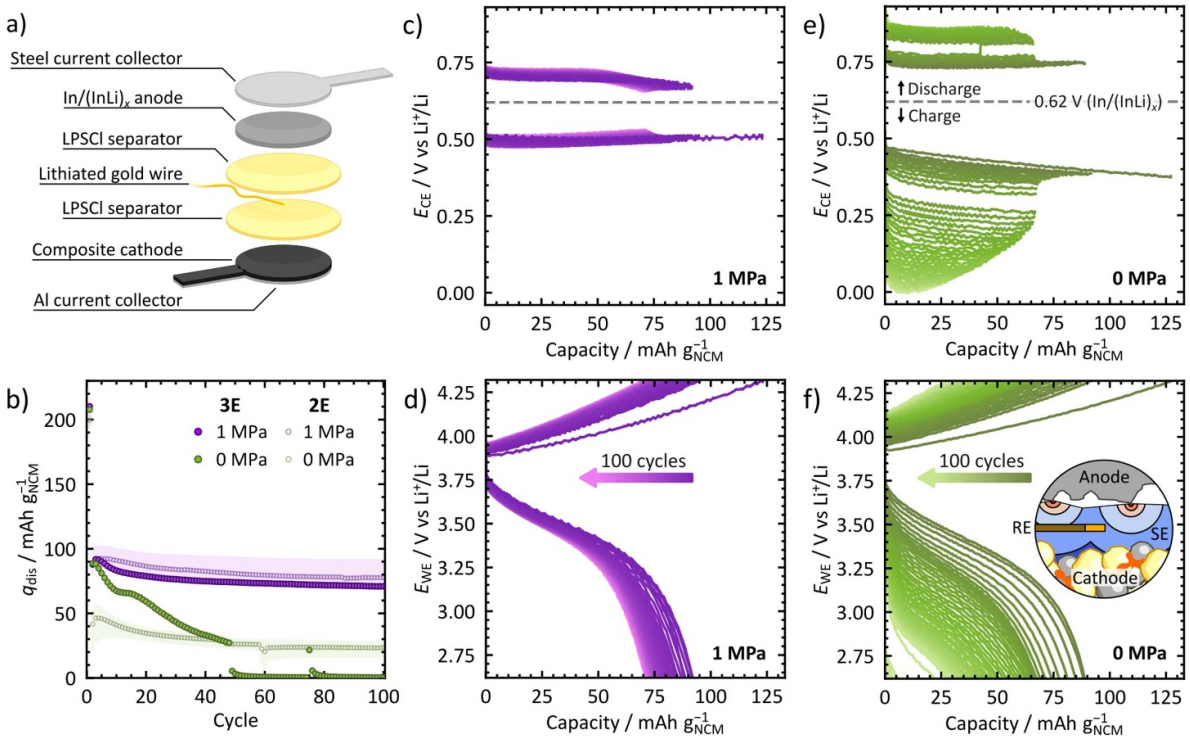

Figure 7. Long-term cycling of 3E In/InLi|LPSCl|NCM pouch cells with a stack pressure of 1 MPa (violet) and 0 MPa (green). The colors get lighter for increasing cycle numbers. (a) 3E pouch cell configuration with a gold wire, which serves as reference electrode. (b) Evolution of the discharge capacity during cycling with 1 C for 2E cells and 3E cells. The semi-transparent curves are identical to those shown in Fig. 2. Evolution of the anode potential E_{CE} during cycling at (c) 1 MPa and (e) 0 MPa. The grey dashed line indicates the open circuit potential of the anode vs. Li^+/Li. Evolution of the cathode potential E_{WE} during cycling at (d) 1 MPa and (f) 0 MPa. The temperature was 25 °C and the areal capacity was 2 mAh cm^{-2}. The inset in (f) schematically displays the proposed electrochemical potential distribution inside the separator upon anode contact loss.

When the pressure is subsequently increased back to 25 MPa, the capacity partially recovers but does not return to its original levels, indicating chemo-mechanical degradation at low pressures. At higher pressures, the difference lessens as interfacial contact within the composite is to some extent restored. To assess the impact of cycling at low pressure, a similar measurement was performed, except that an additional formation cycle, i.e. charging to a high SoC, was conducted at 1 MPa (see Fig. 6b). The formation cycle at 1 MPa results in a capacity drop of 25 mAh g^{-1} in the subsequent 1 C cycle and the capacity remains considerably lower even after increasing the pressure back to 25 MPa. This underscores the irreversible damage caused by reaching a high SoC at low pressures. Consequently, optimized protocols for stable low-pressure cycling may require a reduced cut-off potential of e.g. 4.2 V vs. Li^+/Li to circumvent the H_2–H_3 transformation in Ni-rich NCM, as demonstrated by Gao et al., thereby mitigating the associated significant volume change.[15]

While an elevated temperature of 40 °C results in an overall higher capacity, the profile of the curve is not significantly affected upon pressure reduction from 25 MPa to 1 MPa, and the relative capacity decrease is comparable to that at 25 °C. The capacity drop caused by the formation cycle at 1 MPa is, however, slightly reduced, as impeded charge transport due to a degraded microstructure is partially compensated by a higher ionic conductivity.[53]

Deconvolution of anode and cathode contributions via three-electrode pouch cells.—To identify the main driver for capacity fading observed with the pouch cells at low stack pressure, three-electrode (3E) pouch cells were assembled using a gold wire as a reference electrode (Fig. 7a).[43] For this, the wire was lithiated for 12 h to form a Li–Au alloy, providing a stable potential of 0.31 V vs. Li^+/Li (see Fig. S12). Here, cathode and anode correspond to working electrode (WE) and counter electrode (CE), respectively. Figure 7b shows the long-term cycling performance of two 3E cells cycled at 1 MPa and 0 MPa in comparison with the capacities of the corresponding two-electrode (2E) cells. At 1 MPa the 3E cell reaches a capacity of approximately 90 mAh g^{-1} in the initial cycles, which decreases to 70 mAh g^{-1} after 100 cycles. These values are consistent with the 2E cells, suggesting no substantial contribution of the anode to the overall cell overpotential and long-term cycling stability at 1 MPa. This is confirmed by the potential profiles of the anode potential E_{CE} (see Fig. 7c), which show an overpotential of 80–140 mV relative to the *open circuit potential* (620 mV vs. Li^+/Li) during charge and discharge, in good agreement with the expected Ohmic drop across the separator layer (90 mV, as estimated from EIS measurements, see Fig. S13). Over 100 cycles, the anode overpotential remains relatively stable, whereas a changing cathode potential E_{WE} results in a rather weak but continuous capacity fading (see Fig. 7d). These observations are in line with 3E impedance data obtained before and after long-term cycling at 1 MPa (see Fig. S13). Here, the cathode impedance increases, while anode impedance remains relatively stable.

Without stack pressure, the 3E cell and the 2E cells show more pronounced differences. While the 2E cells deliver a capacity of approximately 50 mAh g^{-1} in the initial cycles, the 3E cell reaches 90 mAh g^{-1}, indicating significant anode-related capacity losses at 0 MPa. In the subsequent cycles, the capacity of the 3E cell diminishes rapidly before approaching comparable values like the 2E cells after 50 cycles, followed by an abrupt drop to 0 mAh g^{-1}. This accelerated capacity fading may be attributed to more severe chemo-mechanical degradation of the cathode as higher SoCs are reached compared to the 2E cells. Both potentials, E_{WE} and E_{CE}, change significantly, and particularly, the anode overpotential increases drastically compared to 1 MPa (see Figs. 7e and 7f), which confirms that the In/(InLi)$_x$ anode is not suitable for measurements without

stack pressure. Moreover, E_{CE} approaches 0 V vs. Li^+/Li suggesting lithium plating, which facilitates dendrite formation and may be the reason for the abrupt cell failure after 50 cycles. The corresponding 3E impedance data before and after long-term cycling confirms a significantly increased cathode and anode contribution after cycling (see Fig. S13).

Importantly, it is likely that the chemo-mechanics of the anode indirectly affect the mechanical degradation of the cathode, as proposed by Kang et al.[54] Moreover, it is likely that the measured cathode potential is affected by the severe contact loss of the anode (or close to the anode) at 0 MPa stack pressure.[49,50] For only a small fraction of remaining anode|separator contacts, the main driver for the measured potential drop on the anode side is likely current focusing. In the case of near-complete delamination of the anode, where the lateral distance between contact spots comes close to the distance between the anode and the reference electrode, the reference electrode potential is significantly affected (as sketched in Fig. 7f), distorting the *apparent* cathode potential.

In Fig. S14 of the Supporting Information, we show the reproducibility of the 3E measurements. Moreover, we provide cycling data of a 3E cell at 1 MPa for 250 cycles at 1 C with intermediate formation cycles. A stepwise capacity decrease is observed after each formation cycle, confirming the detrimental effect of high SoCs and corroborating the findings from the measurements under variable stack pressures using the automatic press.

Based on these findings, we conclude that at a low stack pressure of 1 MPa (and above) capacity fading is predominantly caused by cathode degradation. However, in the here tested pouch cells the capacity fading is rather weakly pronounced, and stable cell operation is possible as mechanical stabilization of the composite microstructure may be promoted by the binder. Although the detrimental effect of insufficient stack pressure on metal anode performance is widely reported and corroborated by our press cell data,[16,42,55] the In/$(InLi)_x$ anode remains relatively stable even at a low stack pressure of 1 MPa and 1 C. However, as mentioned before, it is likely that the observed capacity fading on the cathode side is indirectly affected by chemo-mechanics of the In/$(InLi)_x$ anode. Completely removing stack pressure results in a rapidly increasing anode overpotential upon cycling, linked to anode|separator contact loss (revisit Fig. 5), rendering the In/$(InLi)_x$ anode unsuitable for pouch cell operation without or at extremely low stack pressure.

Conclusions

In this study, we demonstrate significant differences in the low-pressure cycling performance between lab-scale press cells and pouch cells. While comparable electrochemical performance is achieved at higher pressures (25 MPa), pouch cells exhibit a substantially improved performance at low stack pressures (1 MPa and zero stack pressure). Cross-sectional SEM images together with 3E pouch cell measurements reveal that capacity fading under zero stack pressure is dominated by contact loss at the anode|separator interface. In press cells, stack pressures in the low MPa range are not sufficient to prevent contact loss, as internal friction may reduce the pressure effectively experienced within the cell. In pouch cells, by contrast, the In/$(InLi)_x$ anode proves to be a viable option at a stack pressure of 1 MPa. By employing the stable In/$(InLi)_x$ anode, we demonstrate that the sheet-type cathode undergoes only minor capacity fading at this pressure, suggesting a potentially stabilizing role of the binder in mitigating chemo-mechanical degradation. Overall, our results demonstrate that the assessment of low-pressure performance of SSBs can be highly sensitive to the chosen cell configuration. While conventional lab-scale press cells are well suited for probing intrinsic material properties and performance limits at high stack pressure, their application at low stack pressure can lead to underestimation of SSB performance capability. Accurate assessments require cell architectures that mirror targeted designs for practical applications. We therefore suggest (lab-scale) pouch cell configurations as a much more reliable platform for assessing the low-pressure performance of SSBs.

Acknowledgment

We acknowledge financial support within the FestBatt Cluster of Competence (BMFTR, Bundesministerium für Forschung, Technologie und Raumfahrt) in the projects 03XP0430A, 03XP0433D, and 03XP0428E. We acknowledge the German Research Foundation (DFG) POLiS Cluster of Excellence (Project ID 390874152) for financing of the CompreDrive (rhd) device. We acknowledge financial support within the FoFeBat4 project 03XP0590D and FLiPS project 03XP0261 (BMFTR, Bundesministerium für Forschung, Technologie und Raumfahrt). J.K.E. and A.B. acknowledge financial support from the Hessian State Ministry of Higher Education, Research, and the Arts (HMWK). S.S.M.J. and K.B. acknowledge financial support from the Mechano-chemical Understanding of Solid Ion Conductors, an Energy Frontier Research Center funded by the U.S. Department of Energy Office of Science, Office of Basic Energy Science under Grant Nos. DE-SC00234.

Data availability statement

The data presented in this work including electrochemical cycling data is available at: "JLUPub" at https://doi.org/10.22029/jlupub-21003.

ORCID

J. Schubert https://orcid.org/0009-0003-3148-6672
S. Kremer https://orcid.org/0009-0009-3739-8749
J. Hubl https://orcid.org/0009-0001-5475-5244
P. Minnmann https://orcid.org/0000-0002-9646-0487
F. Rossi https://orcid.org/0009-0004-7134-094X
S. S. M. Ji https://orcid.org/0000-0001-8496-1017
F. H. Richter https://orcid.org/0000-0002-6587-7757
K. Hatzell https://orcid.org/0000-0002-5222-7288
J. K. Eckhardt https://orcid.org/0000-0002-2799-0599
A. Bielefeld https://orcid.org/0000-0003-2193-8375
J. Janek https://orcid.org/0000-0002-9221-4756

References

1. J. Janek and W. G. Zeier, "A solid future for battery development." *Nat. Energy*, **1**, 16141 (2016).
2. J. Janek and W. G. Zeier, "Challenges in speeding up solid-state battery development." *Nat. Energy*, **8**, 230 (2023).
3. Y.-G. Lee et al., "High-energy long-cycling all-solid-state lithium metal batteries enabled by silver–carbon composite anodes." *Nat. Energy*, **5**, 299 (2020).
4. S. Cangaz, F. Hippauf, F. S. Reuter, S. Doerfler, T. Abendroth, H. Althues and S. Kaskel, "Enabling high-energy solid-state batteries with stable anode interphase by the use of columnar silicon anodes." *Adv. Energy Mater.*, **10**, 2001320 (2020).
5. D. H. S. Tan, Y. S. Meng and J. Jang, "Scaling up high-energy-density sulfidic solid-state batteries: a lab-to-pilot perspective." *Joule*, **6**, 1755 (2022).
6. X. Hu et al., "External-pressure–electrochemistry coupling in solid-state lithium metal batteries." *Nat. Rev. Mater.*, **9**, 305 (2024).
7. R. Ruess, S. Schweidler, H. Hemmelmann, G. Conforto, A. Bielefeld, D. A. Weber, J. Sann, M. T. Elm and J. Janek, "Influence of NCM particle cracking on kinetics of lithium-ion batteries with liquid or solid electrolyte." *J. Electrochem. Soc.*, **167**, 100532 (2020).
8. N. Kamaya et al., "A lithium superionic conductor." *Nat. Mater.*, **10**, 682 (2011).
9. A. Sakuda, A. Hayashi and M. Tatsumisago, "Sulfide solid electrolyte with favorable mechanical property for all-solid-state lithium battery." *Sci. Rep.*, **3**, 2261 (2013).
10. M. Papakyriakou, M. Lu, Y. Liu, Z. Liu, H. Chen, M. T. McDowell and S. Xia, "Mechanical behavior of inorganic lithium-conducting solid electrolytes." *J. Power Sources*, **516**, 230672 (2021).
11. R. Koerver, I. Aygün, T. Leichtweiß, C. Dietrich, W. Zhang, J. O. Binder, P. Hartmann, W. G. Zeier and J. Janek, "Capacity fade in solid-state batteries: interphase formation and chemomechanical processes in nickel-rich layered oxide cathodes and lithium thiophosphate solid electrolytes." *Chem. Mater.*, **29**, 5574 (2017).

12. P. Minnmann et al., "Designing cathodes and cathode active materials for solid-state batteries." *Adv. Energy Mater.*, **12**, 2201425 (2022).
13. Q. Li, H. Liu, Y. Ye, K. J. Li, F. Wu, L. Li and R. Chen, "The critical importance of stack pressure in batteries." *Nat. Energy* **10**, 1 (2025).
14. S. Puls et al., "Benchmarking the reproducibility of all-solid-state battery cell performance." *Nat. Energy*, **9**, 1 (2024).
15. X. Gao et al., "Solid-state lithium battery cathodes operating at low pressures." *Joule*, **6**, 636 (2022).
16. T. Krauskopf, H. Hartmann, W. G. Zeier and J. Janek, "Toward a fundamental understanding of the lithium metal anode in solid-state batteries—an electrochemo-mechanical study on the garnet-type solid electrolyte $Li_{6.25}$ $Al_{0.25}$ La_3 Zr_2 O_{12}." *ACS Appl. Mater. Interfaces*, **11**, 14463 (2019).
17. S.-Y. Ham et al., "Assessing the critical current density of all-solid-state Li metal symmetric and full cells." *Energy Storage Mater.*, **55**, 455 (2023).
18. J. Becker, T. Fuchs, T. Ortmann, S. Kremer, F. H. Richter and J. Janek, "Microstructure of lithium metal electrodeposited at the Steel|Li_6PS5Cl interface in 'anode-free' solid-state batteries." *Adv. Energy Mater.*, **15**, 2404975 (2025).
19. T. Krauskopf, F. H. Richter, W. G. Zeier and J. Janek, "Physicochemical concepts of the lithium metal anode in solid-state batteries." *Chem. Rev.*, **120**, 7745 (2020).
20. J. Doux, H. Nguyen, D. H. S. Tan, A. Banerjee, X. Wang, E. A. Wu, C. Jo, H. Yang and Y. S. Meng, "Stack pressure considerations for room-temperature all-solid-state lithium metal batteries." *Adv. Energy Mater.*, **10**, 1903253 (2020).
21. S. Kremer, C. D. Alt, L. Schuster, J. Westphal, B. Aktekin, J. Janek and J. K. Eckhardt, "SEI formation in sulfide-based solid-state batteries: influence of contact conditions on impedance-derived interphase growth kinetics." *ACS Appl. Mater. Interfaces*, **18**, 33450 (2026).
22. M. Yamamoto, Y. Terauchi, A. Sakuda, A. Kato and M. Takahashi, "Effects of volume variations under different compressive pressures on the performance and microstructure of all-solid-state batteries." *J. Power Sources*, **473**, 228595 (2020).
23. D. H. S. Tan et al., "Carbon-free high-loading silicon anodes enabled by sulfide solid electrolytes." *Science*, **373**, 1494 (2021).
24. H. Huo, M. Jiang, Y. Bai, S. Ahmed, K. Volz, H. Hartmann, A. Henss, C. V. Singh, D. Raabe and J. Janek, "Chemo-mechanical failure mechanisms of the silicon anode in solid-state batteries." *Nat. Mater.*, **23**, 543 (2024).
25. K. G. Naik, M. K. Jangid, B. S. Vishnugopi, N. P. Dasgupta and P. P. Mukherjee, "Interrogating the role of stack pressure in transport-reaction interaction in the solid-state battery cathode." *Adv. Energy Mater.* **15**, 2403360 (2024).
26. C. Doerrer, X. Gao, J. Bu, S. Wheeler, M. Pasta, P. G. Bruce and P. S. Grant, "Fast-charging all-solid-state battery cathodes with long cycle life." *Nano Energy*, **134**, 110531 (2025).
27. W. Zhang et al., "Interfacial processes and influence of composite cathode microstructure controlling the performance of all-solid-state lithium batteries." *ACS Appl. Mater. Interfaces*, **9**, 17835 (2017).
28. M. A. Thorpe, M. Zhang, D. W. Liao, S. E. Sandoval, Y. Kim, M. T. McDowell, M. D. Thouless and N. P. Dasgupta, "Controlling stack pressure inhomogeneity in anode-free solid-state batteries using elastomeric interlayers." *Matter*, **8**, 101955 (2025).
29. J. Park, J. Jung, S. Yang, D. H. Kim, J. B. Lee, J. A. S. Oh, H. Yang, M. Nashiru, C. Huang and Y. S. Meng, "Realizing low-pressure operation of all-solid-state lithium–sulfur batteries enabled by carbon-coated current collectors." *Adv. Energy Mater.*, **16**, e04272 (2026).
30. Y. J. Nam, D. Y. Oh, S. H. Jung and Y. S. Jung, "Toward practical all-solid-state lithium-ion batteries with high energy density and safety: comparative study for electrodes fabricated by dry- and slurry-mixing processes." *J. Power Sources*, **375**, 93 (2018).
31. C. Wang, J. T. Kim, C. Wang and X. Sun, "Progress and prospects of inorganic solid-state electrolyte-based all-solid-state pouch cells." *Adv. Mater.*, **35**, 2209074 (2023).
32. J. H. Teo, F. Strauss, Đ. Tripković, S. Schweidler, Y. Ma, M. Bianchini, J. Janek and T. Brezesinski, "Design-of-experiments-guided optimization of slurry-cast cathodes for solid-state batteries." *Cell Rep. Phys. Sci.*, **2**, 100465 (2021).
33. T. Y. Kwon, K. T. Kim, D. Y. Oh, Y. B. Song, S. Jun and Y. S. Jung, "Three-dimensional networking binders prepared *in situ* during wet-slurry process for all-solid-state batteries operating under low external pressure." *Energy Storage Mater.*, **49**, 219 (2022).
34. Y. J. Park, K. T. Kim, S. Jun, J. S. Kim, J. Yoon, C. Bak, Y. M. Lee, D. H. Kim, J. Y. Kim and Y. S. Jung, "Multi-faceted binder enhancement via slurry-applicable thiol-ene click chemistry for low-pressure-operable all-solid-state batteries." *Adv. Funct. Mater.*, **36**, e16017 (2026).
35. S.-B. Hong, Y.-R. Jang, H. Kim, Y.-C. Jung, G. Shin, H. J. Hah, W. Cho, Y.-K. Sun and D.-W. Kim, "Wet-processable binder in composite cathode for high energy density all-solid-state lithium batteries." *Adv. Energy Mater.*, **14**, 2400802 (2024).
36. K. Hayashi, T. Mori, C. Beamer and H. Ito, "Effect of process duration on electrochemical performance in composite cathodes for all-solid-state Li-Ion batteries processed via warm isostatic pressing." *ACS Omega*, **11**, 1945 (2025).
37. Y. Chen et al., "Enabling uniform and accurate control of cycling pressure for all-solid-state batteries." *Adv. Energy Mater.*, **14**, 2304327 (2024).
38. K. H. Baeck et al., "Chemo-mechanical failure and reinforcement of solid electrolyte films for practical all-solid-state Li metal pouch cells." *Adv. Mater.*, **38**, e18655 (2026).
39. M. Wolf, B. Vom Hau, R. Wilhelm, M. M. Kaye, A. Stoeckle, J. Kriegler, F. Schmidt, S. Stojcevic, K. Huber and S. Lux, "Impact of extrusion and direct calendering on dry-coated cathodes for sulfidic all-solid-state batteries." *Adv. Energy Mater.*, **16**, e06443 (2026).
40. N.-Y. Park, H.-U. Lee, T.-Y. Yu, I.-S. Lee, H. Kim, S.-M. Park, H.-G. Jung, Y.-C. Jung and Y.-K. Sun "High-energy, long-life Ni-rich cathode materials with columnar structures for all-solid-state batteries." *Nat. Energy*, **10**, 479 (2025).
41. D.-H. Kim, Y.-H. Lee, J.-M. Yoon, P. Thondaiman, B. C. Kim, I.-C. Choi, J.-H. Choi, K.-J. Jeon and C.-M. Park, "Li–Si compound anodes enabling high-performance all-solid-state Li-ion batteries." *Joule*, **9**, 12 (2025).
42. C. Wang et al., "The influence of pressure on lithium dealloying in solid-state and liquid electrolyte batteries." *Nat. Mater.*, **24**, 907–16 (2025).
43. C. Sedlmeier, R. Schuster, C. Schramm and H. A. Gasteiger, "A micro-reference electrode for electrode-resolved impedance and potential measurements in all-solid-state battery pouch cells and its application to the study of indium-lithium anodes." *J. Electrochem. Soc.*, **170**, 030536 (2023).
44. M. Kissel et al., "Quantifying the impact of cathode composite mixing quality on active mass utilization and reproducibility of solid-state battery cells." *Adv. Energy Mater.*, **15**, 2405405 (2025).
45. L. de Biasi, B. Schwarz, T. Brezesinski, P. Hartmann, J. Janek and H. Ehrenberg, "Chemical, structural, and electronic aspects of formation and degradation behavior on different length scales of Ni-rich NCM and Li-Rich HE-NCM cathode materials in Li-ion batteries." *Adv. Mater.*, **31**, 1900985 (2019).
46. D. E. Niesz, "A review of ceramic powder compaction." *KONA Powder Part. J.*, **14**, 44 (1996).
47. B. Azhdar, B. Stenberg and L. Kari, "Determination of springback gradient in the die on compacted polymer powders during high-velocity compaction." *Polym. Test.*, **25**, 114 (2006).
48. A. Diener, S. Ivanov, W. Haselrieder and A. Kwade, "Evaluation of deformation behavior and fast elastic recovery of lithium-ion battery cathodes via direct roll-gap detection during calendering." *Energy Technol.*, **10**, 2101033 (2022).
49. K. G. Naik, D. Chatterjee and P. P. Mukherjee, "Solid electrolyte–cathode interface dictates reaction heterogeneity and anode stability." *ACS Appl. Mater. Interfaces*, **14**, 45308 (2022).
50. D. K. Singh, A. Henss, B. Mogwitz, A. Gautam, J. Horn, T. Krauskopf, S. Burkhardt, J. Sann, F. H. Richter and J. Janek, "Li6PS5Cl microstructure and influence on dendrite growth in solid-state batteries with lithium metal anode." *Cell Rep. Phys. Sci.*, **3**, 101043 (2022).
51. P. Minnmann, J. Schubert, S. Kremer, R. Rekers, S. Burkhardt, R. Ruess, A. Bielefeld, F. H. Richter and J. Janek, "Editors' choice—visualizing the impact of the composite cathode microstructure and porosity on solid-state battery performance." *J. Electrochem. Soc.*, **171**, 060514 (2024).
52. J. Schubert, P. Minnmann, S. Kremer, J. K. Eckhardt, A. Bielefeld and J. Janek, "Evaluating the pressure dependence of charge transport in composite cathodes for solid-state batteries." *ACS Electrochem.*, **2** (2026).
53. P. Minnmann, L. Quillman, S. Burkhardt, F. H. Richter and J. Janek, "Editors' choice—quantifying the impact of charge transport bottlenecks in composite cathodes of all-solid-state batteries." *J. Electrochem. Soc.*, **168**, 040537 (2021).
54. J. Kang, H. R. Shin, J. Yun, S. Kim, B. Kim, K. Lee, Y. Lim and J.-W. Lee, "Chemo-mechanical failure of solid composite cathodes accelerated by high-strain anodes in all-solid-state batteries." *Energy Storage Mater.*, **63**, 103049 (2023).
55. J. Kasemchainan, S. Zekoll, D. S. Jolly, Z. Ning, G. O. Hartley, J. Marrow and P. G. Bruce, "Critical stripping current leads to dendrite formation on plating in lithium anode solid electrolyte cells." *Nat. Mater.*, **18**, 1105 (2019).